Experimental and numerical study using LES of Laser Ignition in a Rocket Like Configuration

G. Lacaze[1], B. Cuenot[1], T. Poinsot[1,2] and M. Oschwald[3]

[1] *CERFACS, 42 Avenue G. Coriolis, 31057 Toulouse cedex, France.*
[2] *Institut de Mécanique des Fluides de Toulouse, Avenue C. Soula, 31400 Toulouse, France.*
[3] *DLR Lampoldshausen, 74239 Hardthausen, Germany.*

Abstract

This paper describes a joint numerical and experimental study of a violent ignition sequence in a laboratory- scale H2-O2 rocket chamber ignited by a laser. Schlieren views and pressure measurements allow to follow the flame propagation experimentally. The LES includes shock capturing, a 6 species - 7 reactions for H2-O2 and a new model for energy deposition by a laser. The flame/turbulence interaction model is the thickened flame model. LES is used to compute the filling phase (where the chamber is filled with hydrogen and oxygen) and the ignition phase. The flame positions observed experimentally and numerically agree as well as the pressure curves in the chamber, showing that LES has the capacity to predict ignition sequences in rocket engines.

Keywords: Ignition, numerical combustion, rocket engines

1. Introduction

Large Eddy Simulation (LES) is a powerful tool to study unsteady complex flows. The concept of explicitely solving for the large geometry-dependent turbulent scales while modelling the dissipative behavior of the smaller scales, combined with high order numerical schemes and optimized unstructured meshes, has already shown its accuracy for gaseous turbulent flows [1–3]. Its recent extension to reacting flows confirmed this potential [4–7] and recent results obtained on burners of gas turbine configurations are very encouraging [8–11]. The application of LES to rocket engines is even more recent and faces specific problems such as high compressibility (including shocks) and very fast chemical reactions [12]. It is however crucial as rocket engines are subjected to critical transient and/or unsteady reacting flows such as ignition and combustion instabilities.
The present paper is a first step towards the application of LES to ignition in rocket engines. The ignition sequence, the compressible nature of the flow (with supersonic inlets) and the fast H2-O2 chemistry require a specific methodology developed herein. The validation is performed on the laser ignition experiment of DLR [13] that reproduces ignition in rocket engine-like conditions.

The paper is organised as follows : section 2 de-

scribes the phenomenology and physics of ignition in rocket engines and section 3 presents the ignition experiment. Section 4 develops the LES methodology for such flows and the numerical approach. Then the simulation is described in section 5 and finally the results are analysed in section 6. Conclusions are given in the last section 7.

2. Ignition of liquid rocket engines

The ignition of liquid rocket engines is a crucial but delicate phase. Due to the very fast injection jets and very fast chemistry the ignition time is the key parameter for the success or fail of ignition : if it is too short, reactants are not sufficiently mixed to sustain combustion and if it is too long, the already mixed reactants ignite strongly with high and dangerous pressure levels.
Three main phenomena control liquid rocket engine ignition : supersonic jets, auto-ignition and H2/O2 combustion. Figure 1 shows a simplified sketch of the system, from the injection plate supporting hundreds of coaxial injectors to the exit nozzle. The ignition of the engine follows a specific sequence. First the system is purged with an inert gas (Helium) to reach a nominal state and to cool down injection lines. Then hydrogen injection starts and after a few milliseconds the igniter is triggered. In real engines, the igniter is either a pyrotechnic system or a cryotechnic burner. The igniter produces a high pressure jet leading to a strongly under-expanded jet in the chamber. Finally the oxidizer (O2) is injected and combustion begins.

3. The M3 burner experiment

The M3 burner experiment operated at the DLR center of Lampoldshausen [13] has been designed to investigate ignition in a rocket like configuration, and more specifically the effect of injection conditions on the ignition sequence. Ignition is triggered thanks to a Nd:YAG ($\lambda = 532\ nm$) laser beam. Different injection regimes have been tested, resulting in multiple ignition sequences [13]. The selected test case corresponds to a strong ignition (high maximum pressure), with a long intake phase that fills the chamber with a H2-O2 gaseous flammable mixture before laser ignition. When ignition occurs the flame spreads over the whole chamber very rapidly leading to a sharp pressure peak. Once the mixture is burnt, the flame anchors near the injector lips into a diffusion mode [13].

3.1. Experimental set-up

The test rig is fueled with gaseous hydrogen and oxygen by a coaxial injector and connected to the atmosphere by an exhaust nozzle (Fig. 2). The chamber is a 14 cm long box with a square section (6x6 cm^2) designed to sustain pressures up to 20 bars (Fig. 2). Complete optical access to the chamber volume is obtained via two opposed quartz windows. On the two other sides smaller windows are used to introduce the igniting laser beam. Burnt gases exhaust through a 4 mm diameter nozzle. The coaxial injector is composed of a 1.22 mm diameter O2 injection tube surrounded by a H2 injection annulus with an inner diameter of 2 mm and an outer diameter of 4 mm.

The laser ignites the mixture by an energy deposition of 195 mJ over 10 ns per pulse. The beam is focused in the mixing layer between the reactant jets, at 36 mm downstream the injection plate and at 2.5 mm above the injector axis (Fig. 2b). Schlieren images show that a hot plasma develops within an ellipsoid of 3.5 mm diameter and 2 mm length in the axial direction. No change of the flame behavior has been reported for energy depositions varying between 80 and 195 mJ.

Pressure and temperature probes are placed in the hydrogen and oxygen injection domes to measure their respective total pressures and temperatures (Fig. 2b), and pressure is also measured in the chamber. In addition Schlieren Photography is used to visualize the flow topology and the flame development.

3.2. Experimental conditions

The experiment is operated at room temperature ($\approx 300\ K$) and pressure ($\approx 1.013\ bar$). Mass fluxes of hydrogen and oxygen are estimated thanks to chocked nozzles located upstream of the domes in the injection lines, where pressures and temperatures are measured (Table 1).

In order to define a reference condition, the chamber and the injection lines are purged with N2 before each test (Table 2). Once nitrogen injection is stopped the propellants injection step starts. Hydrogen and oxygen are injected at a mixture ratio of $\dot{m}_{O_2}/\dot{m}_{H_2} = 2$ corresponding to an equivalence ratio of 4. During the propellants injection phase, H2 is first injected alone for 7 ms, then the O2 valve is also opened. The injection phase lasts 370 ms before the laser is triggered.

4. LES of H2/O2 compressible reacting flows

4.1. Explicit compressible LES solver

A fully unstructured solver is used to advance the compressible Navier Stokes equations for a multi-species gas using perfect gas laws [14]. It is based on a finite volume formulation and an explicit integration scheme. Realistic thermochemistry is used, allowing multi-step kinetics for the oxidation of hydrocarbons or hydrogen [15]. For the present calculation, a one-step Runge-Kutta method is employed. Sub-grid scale turbulent viscosity is defined by the Smagorinsky model [16]. Characteristic boundary conditions are set with the NSCBC method [17].

A summary of the LES equations solved by the code is given below [5] :

$$\frac{\partial \overline{\mathbf{w}}}{\partial t} + \nabla \cdot \overline{\mathbf{F}} = \overline{\mathbf{S}}_{\mathbf{c}} \qquad (1)$$

where $\overline{\mathbf{w}}$ is the vector of conservative variables, $\overline{\mathbf{F}}$ is the flux tensor composed of viscous, inviscid and subgrid scale components and $\overline{\mathbf{S}}_\mathbf{c}$ is the chemical source term. $\overline{\mathbf{w}}$ and $\overline{\mathbf{S}}_\mathbf{c}$ are given respectively by :

$$\begin{aligned} \mathbf{w} &= (\rho u, \rho v, \rho w, \rho E, \rho_k)^T \\ \overline{\mathbf{S}}_\mathbf{c} &= (0, 0, 0, \dot{\omega_T} + \dot{Q}, \dot{\omega_k})^T \end{aligned} \quad (2)$$

where ρ is the density, $\mathbf{u} = (u, v, w)^T$ the velocity vector, the total energy per unit mass is defined by $E = \frac{1}{2}\mathbf{u}\cdot\mathbf{u} + E_i$ where E_i is the internal energy, and $\rho_k = \rho Y_k$ where Y_k is the mass fraction of species k. The models for the reaction rates $\dot{\omega_k}$ and the heat release $\dot{\omega_T}$ in Eq. 2 are described in section 4.3. The $\dot{Q}$ is the power deposited by the laser (section 4.5).

4.2. Shock capturing in centered LES scheme

As mentioned in the description of liquid rocket engines ignition (section 2), the conditions of injection lead to supersonic under-expanded jets with shocks in a succession of expansion/recompression cells [18]. This flow structure obviously has an impact on ignition and must be reproduced. To capture the shocks and slip lines present in the flow, the methodology of Cook and Cabot [19] was used. It aims at thickening the shock front by introducing a bulk viscosity β in the viscous stress tensor $\underline{\tau}$:

$$\underline{\tau}_{modified} = (\beta - \frac{2}{3}\mu)\,\nabla.\mathbf{u}\,\underline{\delta} + 2\mu\underline{S} \quad (3)$$

where μ is the dynamic viscosity and $\underline{S}$ is the symmetric strain rate tensor. The bulk viscosity is modeled as :

$$\beta = C(\Delta x)^4 |\nabla^2 \widetilde{S}| \quad (4)$$

where C is fixed to 5. This bulk viscosity acts on the very sharp velocity gradients characterizing shocks but naturally goes back to 0 where the velocity evolves smoothly. Tests have shown that it does not effect the LES quality away from shocks.

4.3. Chemical modeling for LES of H2/O2 combustion

Ignition is a complex chemical process and a seven-step chemical scheme using six species (H2, O2, H2O, OH, O, H) extracted from the work of Baurle [15] is used for the present LES (Table 3). This scheme accurately reproduces the laminar flame speed and adiabatic temperature over a large range of equivalence ratio and takes pressure effects into account. It is also able to predict ignition. No tabulation is used and all species involved in the reactions of Table 3 are explicitly solved by the code. In the experiment the equivalence ratio (ϕ) of the H2/O2 mixture ranges from lean to very rich conditions ($\phi = 4$). Initially, the chamber pressure is about 2 bar and during ignition, the peak pressure reaches 11 bar.

Figure 3 shows the comparison between detailed chemistry [20] and the seven-step scheme for the prediction of the laminar flame speed of premixed laminar flames. The laminar flame velocity is predicted with an error of about 10% around an equivalence ratio of 1.5 but is correct for both lean and rich conditions.

Figure 4 presents the laminar flame velocity plotted versus pressure (at $\phi = 1$) given by the seven-step scheme and compared to three detailed chemistries from Connaire [20], Kee [21] and Smooke [22]. Results show a maximum error of 18% at 10 bar between the seven-step scheme and the three detailed chemistries.

4.4. Flame turbulence interaction model

To handle flame/turbulence interaction, the dynamically thickened flame model (TFLES) is used [9, 23–26]. This model thickens the flame front by a factor F so that it can be resolved on LES grid. The interaction between turbulence and chemistry is modelled through the so-called efficiency function, E [27] which accounts for the influence of the sub-grid scale wrinkling. The TFLES model has been applied successfully in several simulations (premixed and partially premixed) and more details can be found in Ref. [8, 9, 24, 27, 28].

4.5. Laser model for ignition in LES

A specific model (called ED for Energy Deposition) was built to describe the ignition by laser. This model simulates only the effect of the plasma on the surrounding gas and not the plasma itself (Fig. 5). In an electric or a laser spark, ignition does not occur within the plasma but in the unionized mixture in the near vicinity of the hot kernel. With the ED model, the plasma volume is assumed to be null, the energy injected in the calculation domain represents the amount of energy transferred from the plasma to the gaseous mixture. For laser ignition this energy accounts for about 10% of the laser energy [29, 30] (most of the initial energy is lost in the created shock wave). Then the mixture ignites by auto-ignition.

In the ED, the laser is represented by a power $\dot{Q}$ deposited at the beam focus location. This term $\dot{Q}$ is a volumic source term that is directly added to the energy equation 2. The shape of the $\dot{Q}$ term is taken as a gaussian distribution in time and space :

$$\dot{Q}(x, y, z, t) = \frac{\varepsilon_i}{4\pi^2.\sigma_r^3.\sigma_t}.e^{-\frac{1}{2}(\frac{r}{\sigma_r})^2}.e^{-\frac{1}{2}(\frac{t-t_o}{\sigma_t})^2} \quad (5)$$

where r is defined as the distance between a point of space and the laser focus center, t_o is the time when $\dot{Q}$ is maximum, ε_i is the total amount of deposited energy and σ_r and σ_t are the spatial and temporal widths of the deposition.

To capture the very first moments of ignition, the ED model disables flame thickening at the start of ignition and during the formation of the flame kernel, that is mostly a laminar process. Flame thickening is reintroduced when the maximum temperature reaches a crossover value Tc (typically Tc is fixed at 90% of the adiabatic temperature).

The energy deposition is focused at the same location as in the experiment. The shape of the kernel is simplified to a 6 mm diameter sphere, i.e. larger than the real diameter (3.5 mm), to allow a sufficient grid resolution. Similarly the pulse duration is increased to 500 ns (instead of 10 ns) to have a correct time resolution. Finally, the total amount of energy transferred to the mixture is set to 40 mJ, i.e. 20% of the Laser energy. Preliminary tests have shown that the size, duration and energy of the laser shot used in the LES had limited effect on the flame evolution because the laser shot is powerful enough to produce a successful ignition at every test even if the chemical run-away time varies.

5. Numerical configuration

The numerical configuration reproduces the 3D combustion chamber with the H2 dome, the O2 inlet tube and the exit throat (Fig. 6). The H2 dome is included to reproduce the back-flow into the hydrogen injection line observed in the experiment. The oxygen injection is choked before ignition and becomes subsonic afterwards due to the chamber pressure rise. To minimize the impact of the exit boundary condition, the atmosphere around the chamber outlet is also calculated on a coarse mesh appended to the chamber exit. The mesh is refined around the jets at inlet and downwards where the jets mix, develop and are ignited by the laser beam. It is fully unstructured and uses tetrahedral cells (Fig. 6c). It counts around 645,000 nodes, with the smallest cell volume being of the order of 10^{-13} m^3.

5.1. Boundary conditions

A specific difficulty appears in such configurations, where the inlet velocity of a reactant (oxygen in the present case) switches from sonic to subsonic depending on the chamber pressure : the boundary condition must be able to switch accordingly, which is not the case for standard formulations of boundary conditions. The key point is to determine when the boundary condition must switch from subsonic to supersonic (or vice-versa). This can be achieved by calculating the momentum, temperature and pressure at inlet from the total pressure (Pi) in the dome and the chamber pressure (Pc), via isentropic nozzle relations between two reservoirs (with appropriate discharge coefficient : Cd). Then the calculated velocity may be used to determine the flow regime and choose the right boundary condition.

In the present case the oxygen inlet is first supersonic as the oxygen dome is about 12 bars and the chamber is at atmospheric conditions, but after ignition, the chamber pressure increases up to 11 bars and the oxygen inlet goes to subsonic. The transition from supersonic to subsonic occurs when the chamber pressure P_c reaches the value $\left(\frac{2}{\gamma+1}\right)^{\frac{\gamma}{\gamma-1}} P_i$. In this expression γ is the specific heat ratio, averaged on the injection surface.

In supersonic inlet conditions, all variables must be set. The mass flux is :

$$\dot{m} = A.Cd.\rho u_{inj} \tag{6}$$

where A is the throat section of the injector and ρu_{inj} is the product of the density and the axial velocity, defined by [31] :

$$\rho u_{inj} = \frac{P_i}{\sqrt{r.T_i}}\sqrt{\gamma}\left(\frac{2}{\gamma+1}\right)^{\frac{\gamma+1}{2(\gamma-1)}} \tag{7}$$

where T_i and P_i are respectively the total temperature and pressure in the dome. The static temperature and pressure at injection are deduced from isentropic relations :

$$T_{inj} = \frac{2}{\gamma+1}T_i \quad and \quad P_{inj} = \left(\frac{2}{\gamma+1}\right)^{\frac{\gamma}{\gamma-1}} P_i \tag{8}$$

Finally the density is calculated from the perfect gas equation of state.

In subsonic inlet conditions, only mass flux and temperature are imposed through a characteristic treatment (NSCBC) [14, 32]. They are calculated from isentropic relations now involving chamber values :

$$\dot{m} = A.Cd.\rho u_{inj} \tag{9}$$

$$\rho u_{inj} = \frac{P_i}{\sqrt{rT_i}}\left(\frac{P_c}{P_i}\right)^{\frac{1}{\gamma}}\sqrt{\frac{2\gamma}{\gamma-1}\left(1-\left(\frac{P_c}{P_i}\right)^{\frac{\gamma-1}{\gamma}}\right)} \tag{10}$$

$$T_{inj} = \frac{2}{\gamma+1}\left(1+\frac{\gamma-1}{2}M^2\right)T_i \tag{11}$$

where M is the Mach number at the injection surface.

At hydrogen inlet the flow remains subsonic during the experiment. A characteristic treatment is used to set the subsonic mass flow rate and the static temperature (Tab. 1). These conditions are imposed at the H2 dome inlet (see Fig. 6).

The exit surface (which is located outside the chamber, in the free atmosphere) is relaxed to the ambiant pressure using NSCBC [14, 32]. The walls in the injection lines and in the exhaust nozzle are adiabatic slip walls, whereas the chamber walls are treated with laws of the wall. The wall temperature is fixed at 300 K.

5.2. Initial conditions

The computation of the ignition sequence is performed in two steps. The first phase is the filling of

the chamber initially full of nitrogen. Then the propagation of the flame is computed in a second phase. Most of the filling phase (from 0 to 368 ms) is computed on a coarse mesh (39,000 nodes) and only the last instants (from 368 to 370 ms) are computed on the fine mesh (Fig. 6c) to establish the small scale structures and the mixture state prior ignition.

6. Results and discussion

6.1. The filling phase

The instantaneous axial velocity field obtained by LES at the end of the filling phase shows recirculation zones starting at the corners of the chamber and developing downwards around the jets. Results show that nearly all the nitrogen has been purged : the remaining N2, mostly trapped in the recirculation zones, has a maximum mass fraction of the order of 0.17. The reactants are well mixed in most of the chamber (the average mixture equivalence ratio is four) and segregation appears only in the vicinity of the inlet. Before ignition the outlet nozzle is chocked and the chamber pressure is equal to 1.75 bar. The oxygen dome pressure is 12 bar and the O2 injection jet is underexpanded. Figure 7 shows an instantaneous pressure field at the injector outlet where several cells of expansion/compression are observed.

6.2. Ignition

The solution obtained at the end of the intake phase at 370 ms is ignited and Fig. 8 shows series of snapshots of the fields of density gradient and velocity in the axial direction at three different times ($t = 30, 247, 681\ \mu s$ after ignition). Schlieren photographs taken from experimental results at $35, 250$ and $680\ \mu s$ after ignition are also reported on Fig. 8. The comparison shows that the simulation captures the flame behavior as well as the global flame shapes. Note that in both LES and experiments, the flame wrinkling seems limited and the flame front is rather smooth.

The laser beam impact is located in a segregated zone where the local stoichiometric ratio is around 2 and where the turbulence intensity of the axial fluctuation is about 20% which leads to $u'/S_l \approx 3$ (with u' the root mean square of the velocity fluctuation and S_l the laminar flame speed). In the early time after ignition, the hot gas kernel (at 4120 K) is convected downstream by the jet without being stretched. Then chemical reactions start and as the kernel grows its surface is increasingly wrinkled by turbulence. As the flame expands in all directions, it encounters mixtures with different equivalence ratios : the front propagating towards the walls and the exit burns a mixture at $\phi = 4$ but the front propagating towards the injection jets sees more and more segregated reactants. At $t \approx 370\ \mu s$ due to combustion the chamber pressure becomes higher than the hydrogen dome pressure and chamber mixture back-flows into the injection dome, this phenomenon is observed in the DLR experiment [13]. Near the injection jet the velocity is then negative and the mixture is close to the stoichiometry making the flame accelerate towards the injector. At $t = 681\ \mu s$ the hydrogen dome pressure is still lower than the chamber pressure and the flame is anchored to the injector (see Fig 8i). At this time the chamber is almost completely filled with burnt gas and at about 1 ms, a lifted flame settles into the mixing layer near the injection. After complete combustion of the fuel trapped near the walls, the premixed flame extinguishes in this zone and only the flame stabilised at the injectors remains. The corresponding pressure chamber evolution is presented in Fig. 9 and compared with experiment, showing again a good agreement.

7. Conclusions

A new compressible LES methodology to compute flame ignition and propagation in a rocket engine fueled by oxygen and hydrogen has been derived and tested in the configuration of DLR [13]. This LES includes shocks computation, chocked outlet and a six-specie, seven-step chemical scheme for H2/O2 chemistry.

Results from LES are in good agreement with experimental observations, showing that the simulation captures the right mechanisms for flame ignition, propagation and stabilisation. The LES methodology for such compressible reacting flows, has been successfully used to reproduce violent delayed ignition in rocket engine like conditions.

Acknowledgment

The authors gratefully acknowledge the support of Snecma DMS (Safran group) and of the computing center CINES, as well as DLR for fruitful discussions.

References

[1] P. Moin, K. Squires, W. Cabot, S. Lee, *Phys. Fluids* A 3 (11) (1991) 2746–2757.

[2] M. Lesieur, O. Metais, *Ann. Rev. Fluid Mech.* 28 (1996) 45 – 82.

[3] M. Lesieur, in: O. Métais, J. Ferziger (Eds.), New tools in turbulence modelling, Les Editions de Physique - Springer Verlag, 1997, pp. 1 – 28.

[4] H. Pitsch, L. Duchamp de la Geneste, *Proc of the Comb. Institute* 29 (2002) 2001–2008.

[5] T. Poinsot, D. Veynante, *Theoretical and numerical combustion*, R.T. Edwards, 2nd edition., 2005.

[6] H. Pitsch, *Ann. Rev. Fluid Mech.* 38 (2006) 453–482.

[7] J. Janicka, A. Sadiki, *Proc. of the Combustion Institute* 30 (2004) 537–547.

[8] L. Selle, G. Lartigue, T. Poinsot, R. Koch, K.-U. Schildmacher, W. Krebs, B. Prade, P. Kaufmann, D. Veynante, *Combust. Flame* 137 (4) (2004) 489–505.

[9] P. Schmitt, T. Poinsot, B. Schuermans, K. Geigle, *J. Fluid Mech.* 570 (2007) 17–46.
[10] M. Freitag, J. Janicka, *Proc. of the Combustion Institute* 31 (2007) 1477–1485.
[11] F. Di Mare, W. P. Jones, K. Menzies, *Combust. Flame* 137 (2001) 278–295.
[12] A. Dauptain, *Allumage des moteurs fusée cryotechniques*, Ph.D. thesis, INPT - CERFACS (2006).
[13] V. Schmidt, D. Klimenko, M. Oschwald, *Preliminary results of test case "A" laser ignition tests for coaxial GH2/GO2-Injection*, Tech. rep., DLR, Lampoldshausen (2003).
[14] V. Moureau, G. Lartigue, Y. Sommerer, C. Angelberger, O. Colin, T. Poinsot, *J. Comput. Phys.* 202 (2) (2005) 710–736.
[15] R. A. Baurle, S. Girimaji, *Comb. and Flame* 134 (2003) 131–148.
[16] J. Smagorinsky, *Month. Weath. Rev.* 91 (1963) 99–164.
[17] T. Poinsot, T. Echekki, M. Mungal, *Combust. Sci. Tech.* 81 (1-3) (1992) 45–73.
[18] P. Thompson, *Compressible-fluid dynamics*, McGraw-Hill, 1972.
[19] A. W. Cook, W. H. Cabot, *J. Comput. Phys.* 203 (2005) 379–385.
[20] M. Connaire, H. Curran, J. Simmie, W. Pitz, C. Westbrook, *International Journal of Chemical Kinetics* 36 (11) (2004) 603–622.
[21] R. Kee, J. Warnatz, J. Miller, *A fortran computer code package for the evaluation of gas phase viscosities, conductivities, and diffusion coefficients*, Tech. Rep. SAND83-8209, Sandia National Laboratories (1983).
[22] M. Smooke, M. Koszykowski, *Fully adaptive solutions of one-dimensional mixed initial-boundary value problem with applications to unstable problems in combustion*, Tech. Rep. SAND 83-8219, Sandia National Laboratories (1983).
[23] J.-P. Légier, T. Poinsot, D. Veynante, in: *Summer Program 2000*, Center for Turbulence Research, Stanford, USA, 2000, pp. 157–168.
[24] C. Martin, L. Benoit, Y. Sommerer, F. Nicoud, T. Poinsot, *AIAA Journal* 44 (4) (2006) 741–750.
[25] A. Sengissen, A. Giauque, G. Staffelbach, M. Porta, W. Krebs, P. Kaufmann, T. Poinsot, *Proc. of the Combustion Institute* 31 (2007) 1729–1736.
[26] G. Staffelbach, *Simulation aux grandes échelles des instabilités de combustion dans les configurations multi-brûleurs*, Ph.D. thesis, Institut National Polytechnique de Toulouse (2006).
[27] O. Colin, F. Ducros, D. Veynante, T. Poinsot, *Phys. Fluids* 12 (7) (2000) 1843–1863.
[28] C. Angelberger, F. Egolfopoulos, D. Veynante, *Flow Turb. and Combustion* 65 (2) (2000) 205–22.
[29] D. Bradley, C. Sheppard, I. Suardjaja, R. Woolley, *Combust. Flame* 138 (2004) 55–77.
[30] T. Phuoc, F. White, *Proc. Combust. Inst.* 29 (2002) 1621 – 1628.
[31] S. A. H., *The Dynamics and Thermodynamics of Compressible Fluid Flow*, Wiley, 1953.
[32] T. Poinsot, S. Lele, *J. Comput. Phys.* 101 (1) (1992) 104–129.

8. Tables

cold flow mass fluxes [g/s]	O2	1.135
	H2	0.592
Dome total temperatures [K]	O2	300
	H2	302
Dome total Pressures [bar]	O2	11.7
	H2	2.1
Pressure of the chamber [bar]		1.87

Table 1: Injection conditions for the M3 test case (at ignition time).

N2 valve closure : t_{N2}	-1000ms
H2 valve opening : t_{H2}	0 ms
O2 valve opening : t_{O2}	7 ms
laser ignition : $t_{ignition}$	370 ms

Table 2: Time sequence for the M3 test case.

Reaction	**A**	β	**Ea**
$H + O_2 = O + OH$	3.62E+17	-0.91	1.653E+4
$O + H_2 = H + OH$	1.53E+5	2.67	6.296E+3
$O_2 + H_2 = OH + OH$	5.13E+13	0.00	4.805E+4
$OH + H_2 = H_2O + H$	6.64E+13	0.00	5.155E+3
$OH + OH = H_2O + O$	1.90E+13	0.00	1.091E+3
$H + OH + M = H_2O + M$	6.67E+22	-2.00	0.000
$H + H + M = H_2 + M$	2.20E+18	-1.00	0.000
third body efficiencies : 2.5 for H_2, 16 for H_2O and 1.0 for all other M			
Units : **A :** $[\mathbf{cm^3/mole.sec}]$; **Ea :** $[\mathbf{cal/mole}]$			

Table 3: The seven-step H2-O2 kinetic scheme.

9. Figures

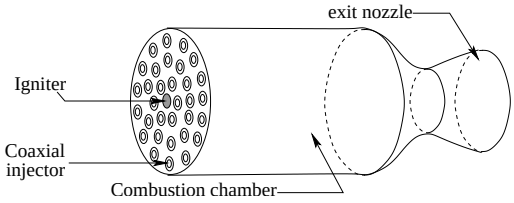

Fig. 1: Sketch of a real combustion chamber.

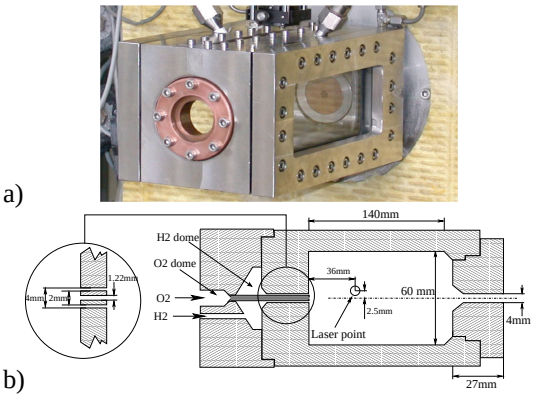

Fig. 2: The Micro-Combustor M3. a) Photograph. b) Geometry.

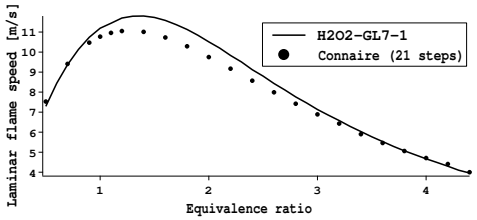

Fig. 3: Chemical comparison of the laminar flame speed given by the seven-step scheme (H2O2-GL7-1) used for the computation and a detailed chemistry from Connaire [20] ($T_{cold\ gas} = 300K$ P=2.0 bar).

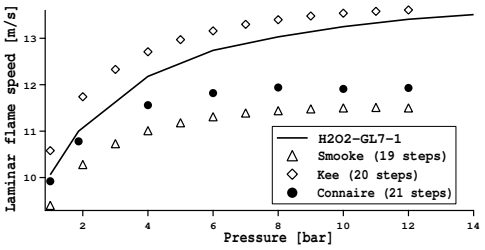

Fig. 4: Laminar flame speed against pressure, comparison between the seven-step scheme (H2O2-GL7-1) and three detailed chemistries from Connaire [20], Smooke [22] and Kee [21] ($T_{cold\ gas} = 300K$, $\phi = 1.0$).

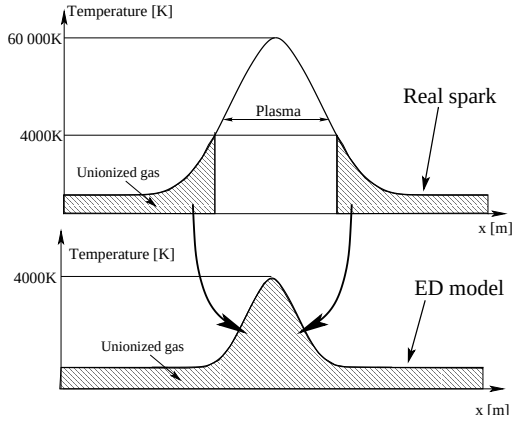

Fig. 5: Sketch of the temperature profile inside a spark kernel and part of the flow modeled with the ED model. With the ED model, only the effect of the plasma on the surrounding unionized gas is simulated.

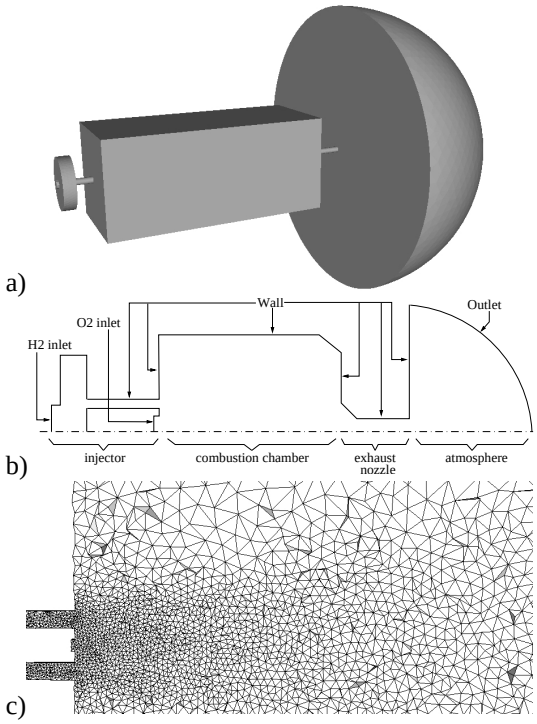

Fig. 6: Computing domain for the M3 Micro-combustor. a) Geometry b) Boundary conditions c) Zoom around the inlet region.

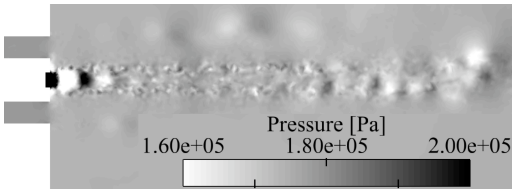

Fig. 7: Pressure field at the injector outlet before ignition.

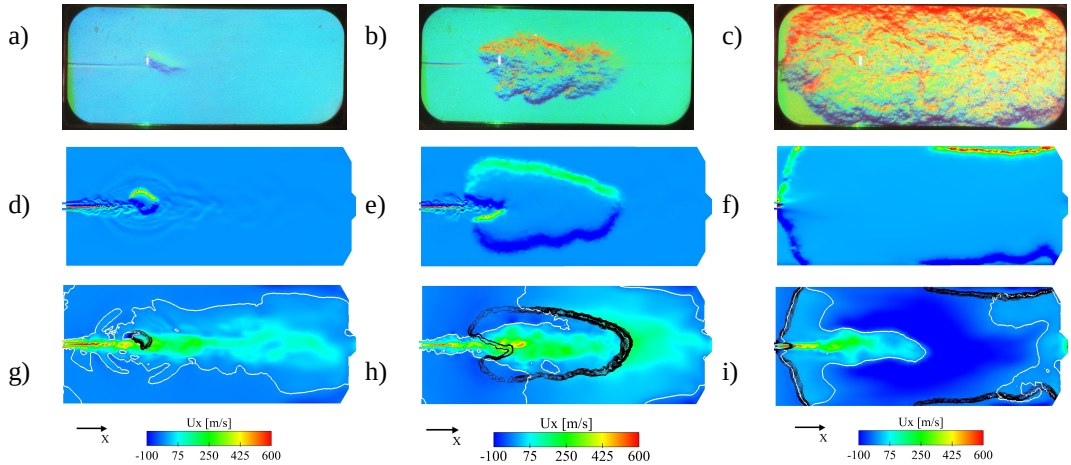

Fig. 8: Schlieren photographs (experiment) at three different times after ignition (a) $t = 35\mu s$, b) $t = 250\mu s$, c) $t = 680\mu s$), snapshots of the density gradient field (LES results) at three different times after ignition (d) $t = 30\mu s$, e) $t = 247\mu s$, f) $t = 681\mu s$) and snapshots of the axial velocity with a Ux = 0 m/s isoline (white) and reaction-rate isolines (black) at three different times after ignition (g) $t = 30\mu s$, h) $t = 247\mu s$, i) $t = 681\mu s$).

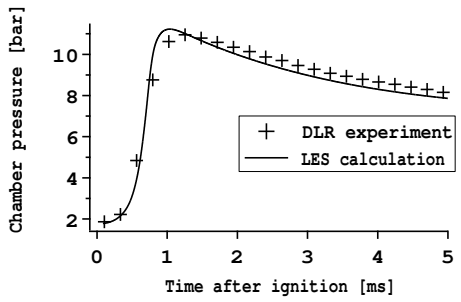

Fig. 9: Temporal evolution of the mean chamber pressure compared with experiment.